

Supporting Information

Endoplasmic reticulum-targeted NIR-II phototherapy combined inflammatory vascular suppression eliciting synergistic effect against TNBC

Guoyun Wan^{*, a}, Xuheng Chen^a, Jiayu Chen^a, Ruiling Gou^a, Haijiao Wang^a, Shuhao Liu^a, Mingyang Zhang^a, Hongli Chen^{a, c}, Dan Wang^{*, b}, Qiqing Zhang^{*, a}

^a *The Key Laboratory of Biomedical Material, School of Life Science and Technology, Xinxiang Medical University, Xinxiang 453003, China*

^b *Xuzhou Central Hospital, Xuzhou 221009, China*

^c *The Third Affiliated Hospital of Xinxiang Medical University, Xinxiang 453003, China*

** Corresponding authors: E-mail: wanguoyun@xxmu.edu.cn; zhangqiq@126.com; wangdan1835324738@163.com.*

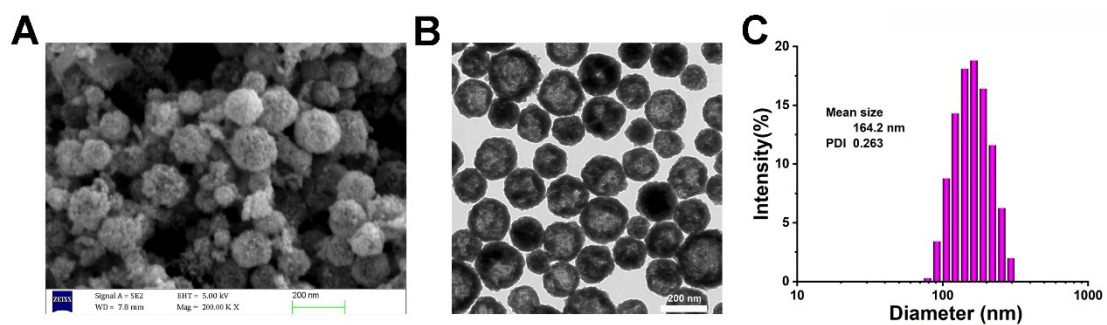


Fig.S1 SEM image (A), TEM image (B) and DLS diameter distribution (C) of $\text{HMCu}_{2-x}\text{S}$.

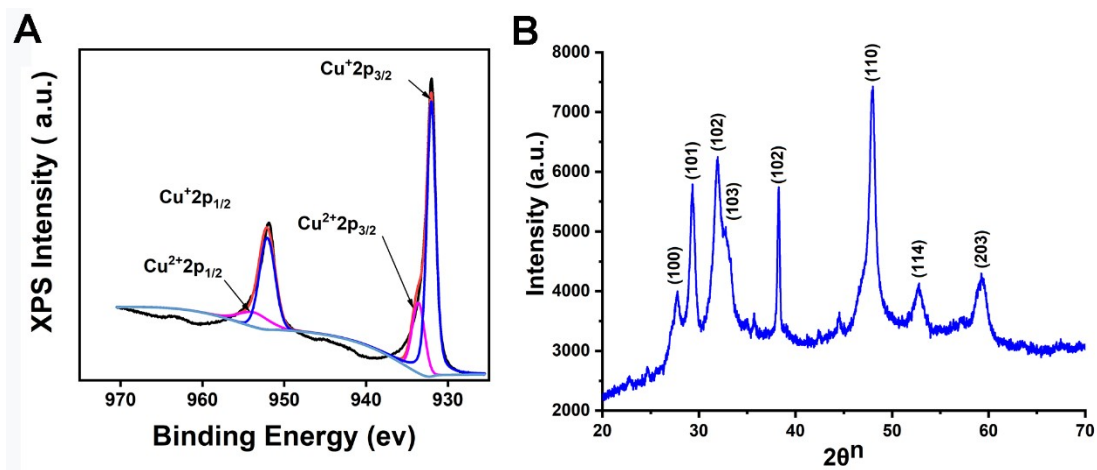


Fig. S2 XPS characterization (A) and XRD characterization (B) of $\text{HMCu}_{2-x}\text{S}$.

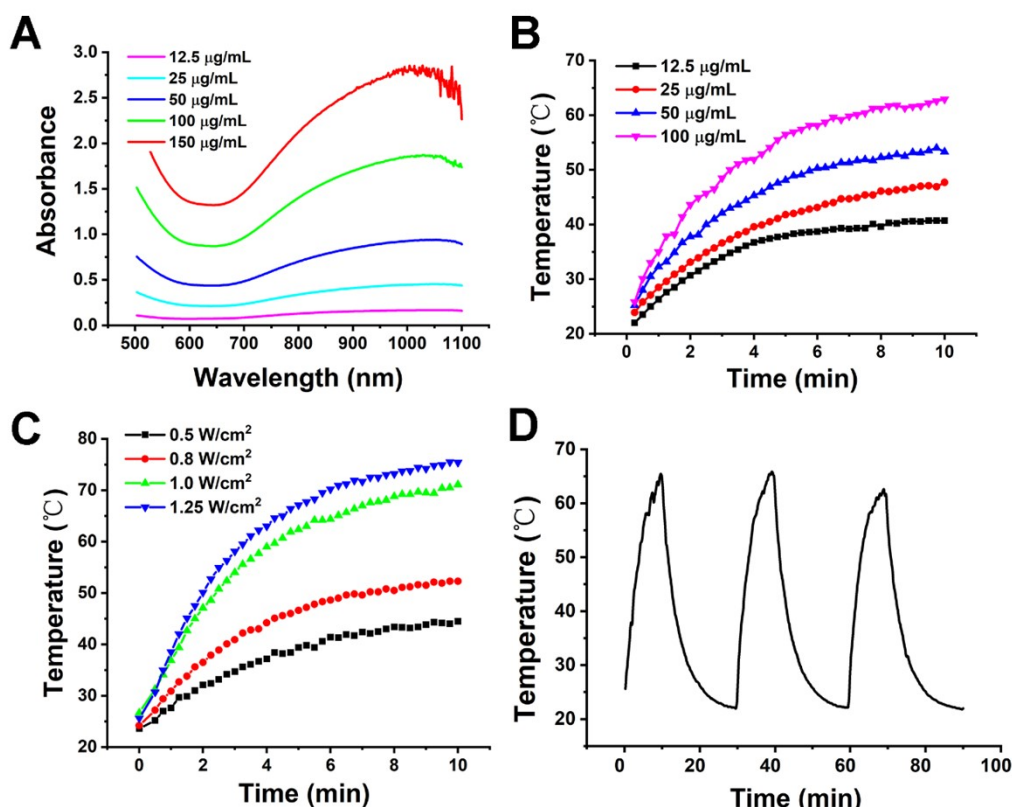


Fig. S3 Photothermal efficiency evaluation of HMCu_{2-x}S. (A) UV-vis spectra of HMCu_{2-x}S dispersions at different concentrations. (B) The temperature change curves of HMCu_{2-x}S dispersions at different concentrations under 1064 nm laser irradiation at 0.8 W/cm² power density. (C) The temperature change curves of 50 µg/mL HMCu_{2-x}S dispersion under 1064 nm laser irradiation in different power intensity. (D) Temperature change curve of 100 µg/mL HMCu_{2-x}S dispersion in three 1064 nm laser irradiation cycles at 0.8 W/cm² power density.

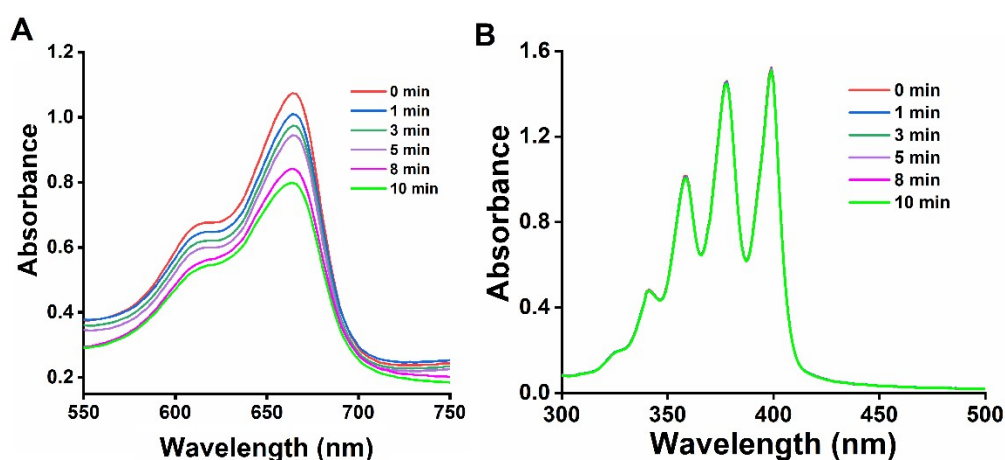


Fig. S4 Irradiation time-dependent UV-vis spectra of the degradation process of MB (A) and ABDA (B) treated with HMCu_{2-x}S under 1064 nm laser irradiation.

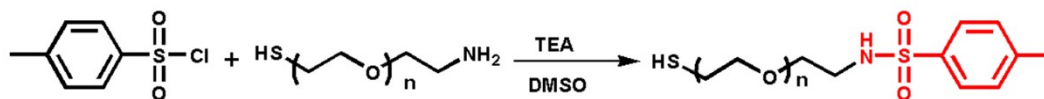


Fig. S5 Synthetic route of the ER-targeted PEG₂₀₀₀.

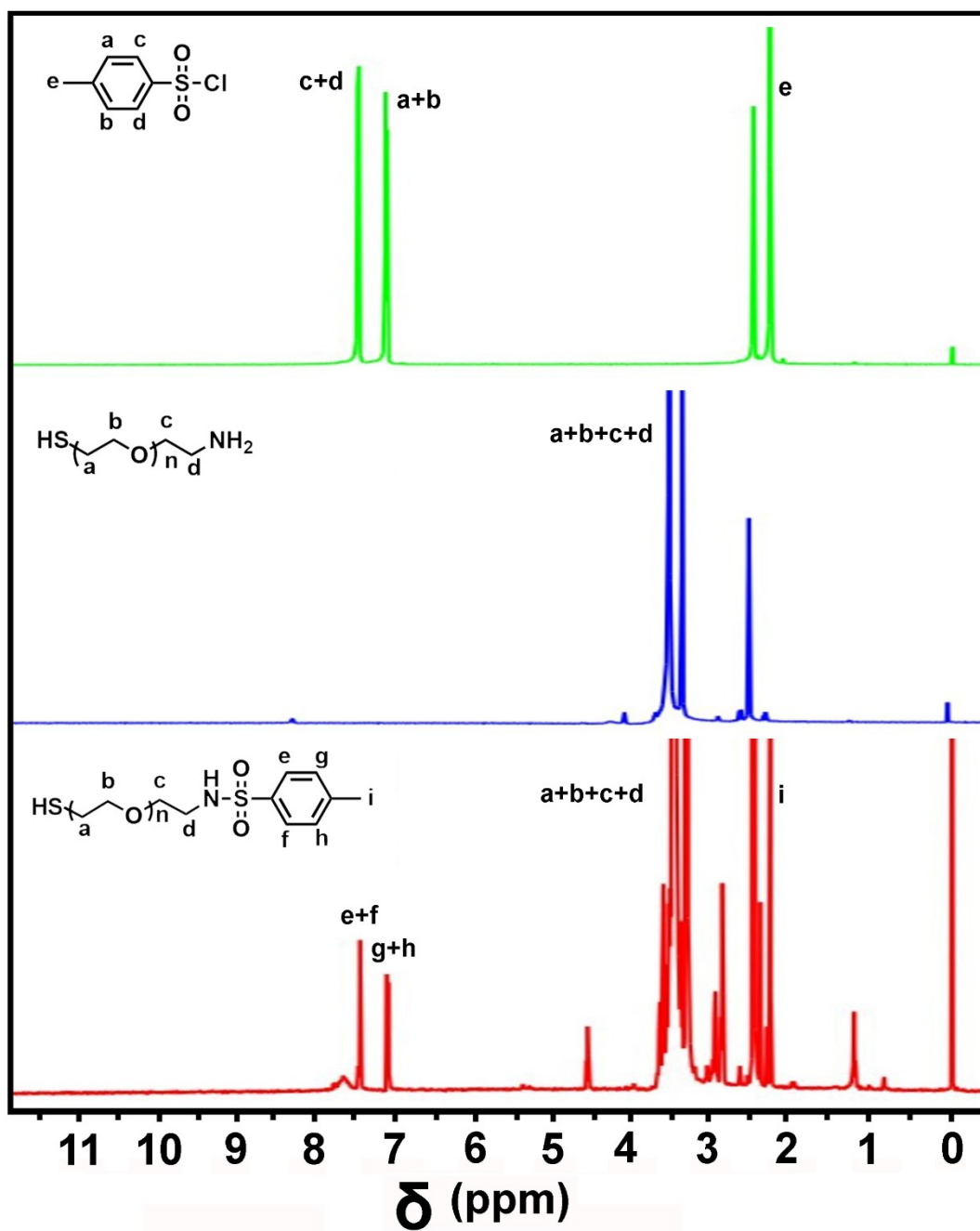


Fig. S6 ¹H NMR spectra of TSC, NH₂-PEG-SH, and ER-PEG-SH.

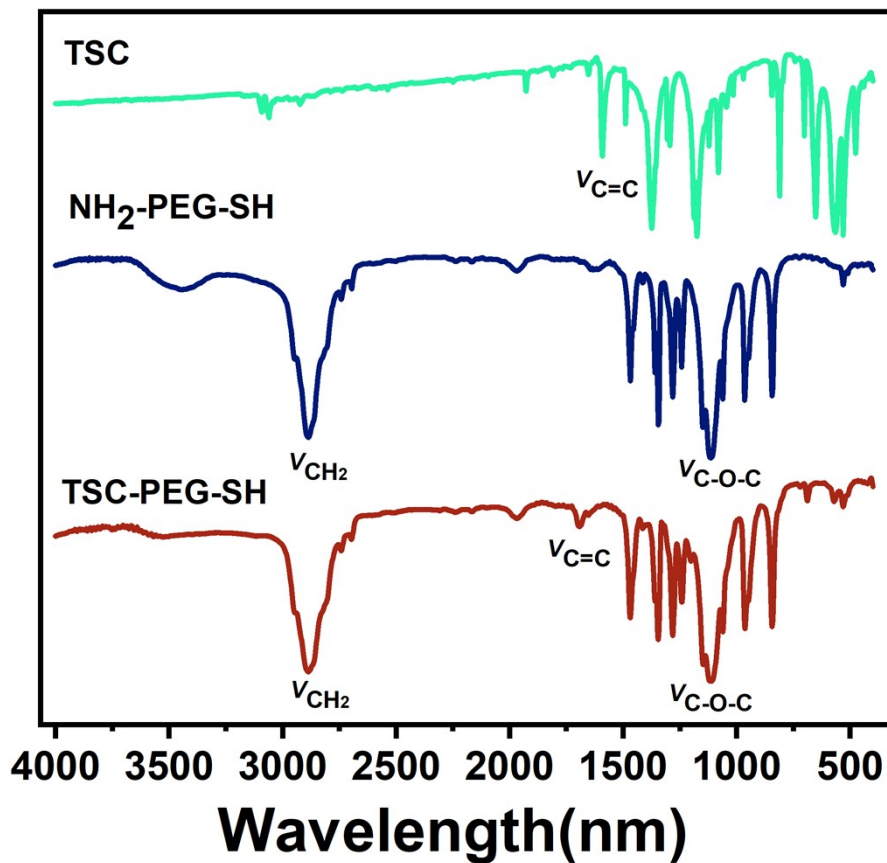


Fig. S7 Fourier transform infrared (FTIR) spectra of TSC, NH₂-PEG-SH and ER-PEG-SH.

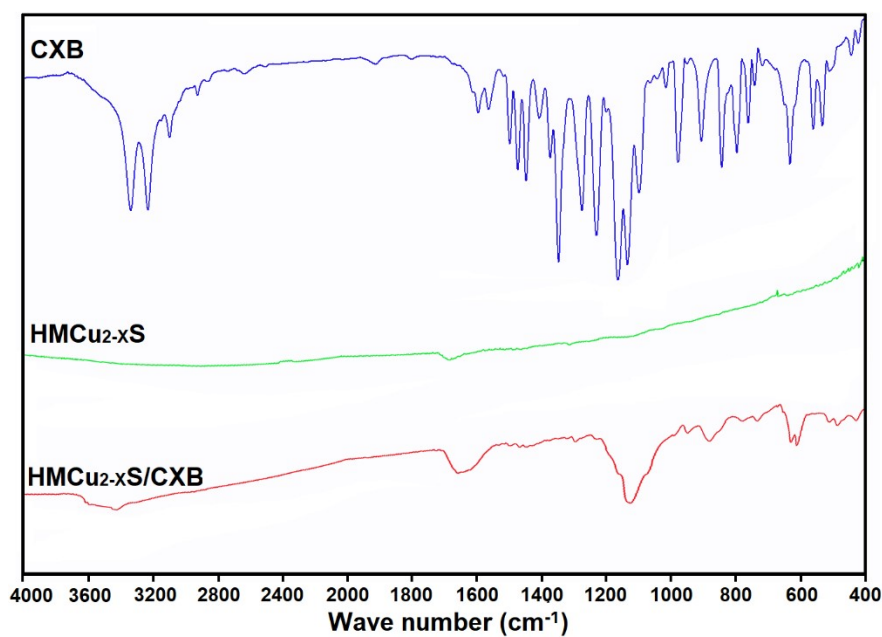


Fig. S8 Fourier transform infrared (FTIR) spectra of CXB, HMCu_{2-x}S and HMCu_{2-x}S/CXB.

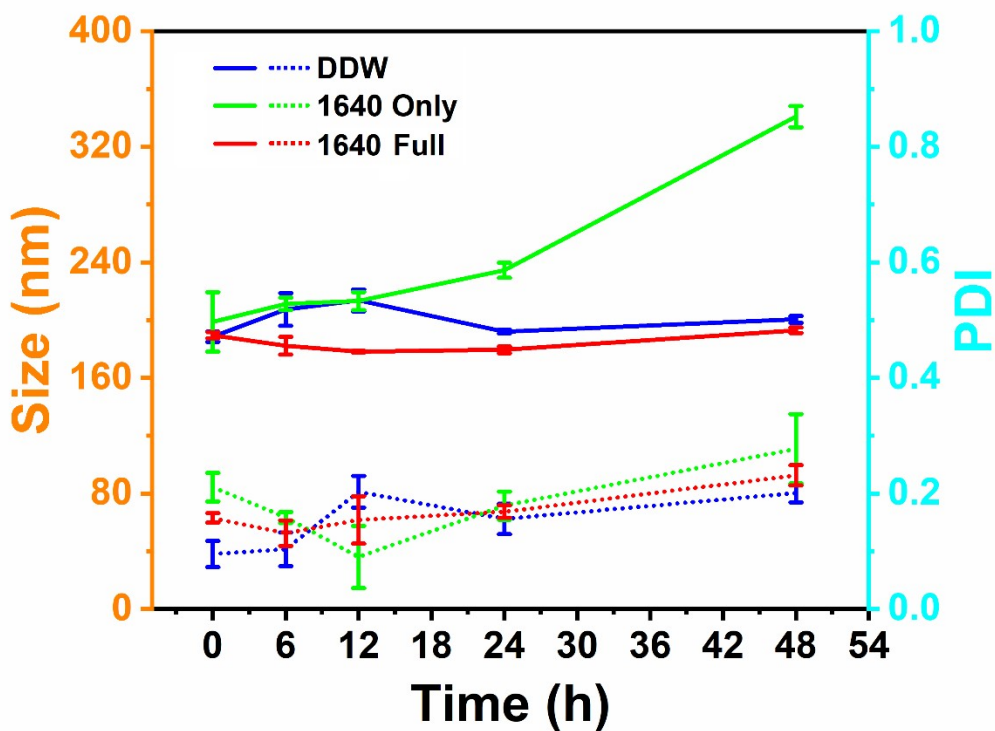


Fig. S9 The size change and PDIs change curves of ER-HMCu_{2-x}S/CXB in different dispersions during 48 h.

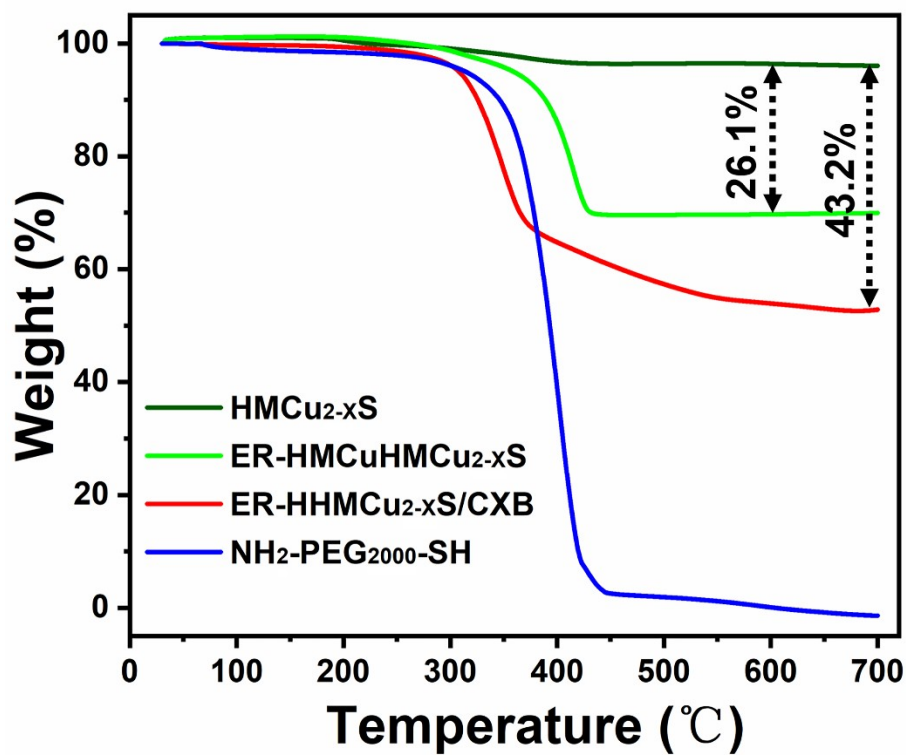


Fig. S10 Thermalgravimetric analysis of HMCu_{2-x}S, ER-HMCu_{2-x}S, ER-HMCu_{2-x}S/CXB and NH₂-PEG₂₀₀₀-SH.

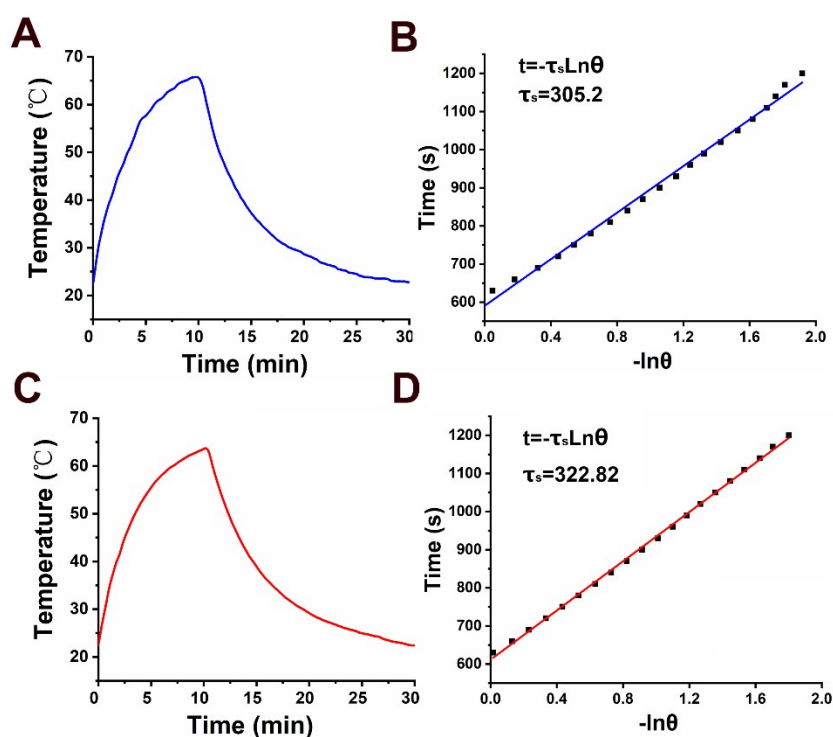


Fig. S11 Temperature change curves of HMCu2-XS (A) and ER-HMCu2-XS/CXB (C) dispersions under 1064 nm irradiation at 0.8 W/cm² during one on/off cycle. Time constant of HMCu2-XS (B) and ER-HMCu2-XS/CXB (D) for heat transfer from the system is determined by applying the linear time data from the cooling period (after 600 s) versus negative natural logarithm of driving force temperature, which is obtained from the cooling stage of (A) and (C).

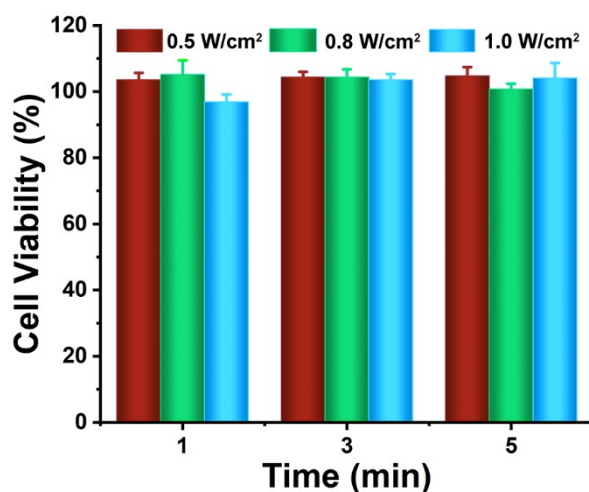


Fig. S12 Cell viability of 4T1 cells after NIR-II laser irradiation with different

conditions.

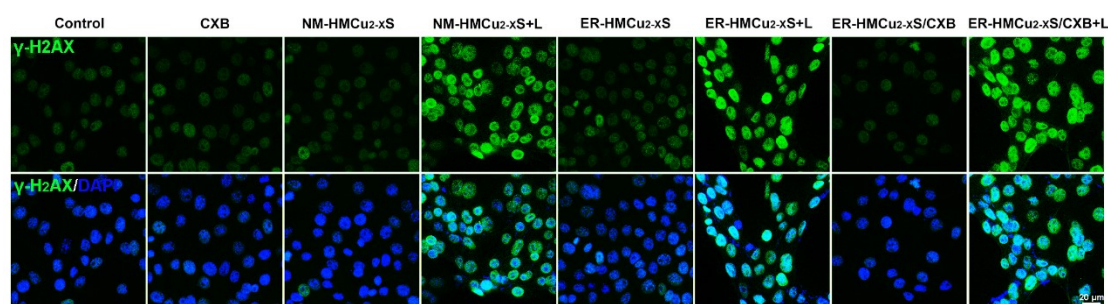


Fig. S13 Immunofluorescence images of 4T1 cells stained with DAPI and γ -H₂AX antibodies after various treatments.

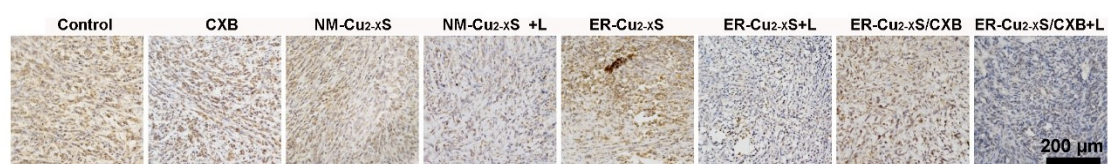


Fig. S14 Immunohistochemical staining images of ki67 in tumor sections after different treatments.

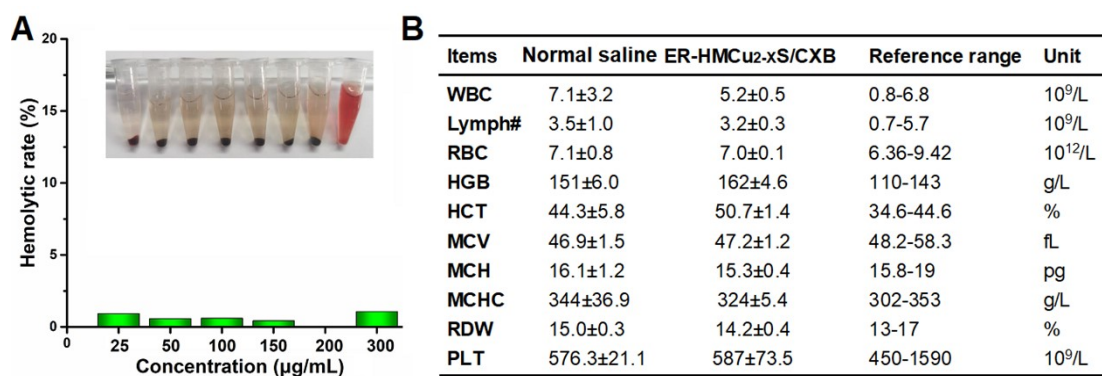


Fig. S15 Preliminary biosafety of ER-HMCu_{2-x}S/CXB. (A) The hemolytic rates of ER-HMCu_{2-x}S/CXB at different concentrations (the insert images show the supernatant of RBCs after incubation). (B) The various major parameters of blood routine test.